Interfacing SFA- and GAM-Type Dynamic Phasors for Modeling of Integrated AC-DC Power Systems

Yingwei Huang, Mehrdad Chapariha, Seyyedmilad Ebrahimi, Navid Amiri, and Juri Jatskevich
Department of Electrical and Computer Engineering
The University of British Columbia
Vancouver, BC, Canada
{ywhuang, mehrdadc, ebrahimi, navida, jurij}@ece.ubc.ca

***Abstract*—This paper focuses on the modeling of integrated ac-dc backup and generation power systems, which has received increasing attention due to the emergence of microgrids and distributed generations. The conventional shifted-frequency analysis (SFA) type dynamic phasors (DPs) assume a bandpass spectrum of power system signals, and thus are only suitable to model system components wherein the 60Hz fundamental frequency is dominant. To account for high-order harmonics of interest in ac-dc systems, this paper considers another type of DPs based on the generalized averaging method (GAM), and proposes a possible interface between the SFA- and GAM-type DP models. Computer studies demonstrate that the proposed DP interface allows for accurate simulations of both fundamental frequency components and high-order harmonics in integrated ac-dc power systems, while providing significant numerical advantages over the conventional time-domain detailed models.**

***Index Terms*—Dynamic phasor, ac-dc system, synchronous machine, rectifier system, harmonics.**

I. Introduction

The rapid development of distributed energy resources (DERs) and smart grid technologies has promoted emergence of modern ac-dc microgrid systems such as one depicted in Fig. 1 [1]. Such systems generally include power sources from utility grid and DERs, different types of loads for various uses, storage elements for demand shaping and short-term supply, some form of backup generation systems supporting medium- to long-term interruptions, various power electronics modules, as well as communications and control infrastructure that integrate all these components. Numerically accurate and efficient modeling of the ac-dc microgrid system components is therefore necessary in all the design, troubleshooting, monitoring, control, and energy management stages.

This paper focuses on the modeling of future integrated ac-dc power generation systems similar to Fig. 1, wherein synchronous machines (SMs) are connected directly to line-commutated rectifiers (LCRs) [2]−[3]. The detailed switch-level models are available in many simulation programs [4]−[8], which require fairly small integration step sizes and often lead to significant increase of the required computing time. Instead of tracking the detailed time-domain waveforms, the so-called dynamic phasor (DP) modeling approaches have been proposed for simulating power system signals in hybrid

This research was supported by the Natural Science and Engineering Research Council (NSERC) of Canada, and was also supported in part by the Institute for Computing, Information and Cognitive Systems (ICICS) at UBC.

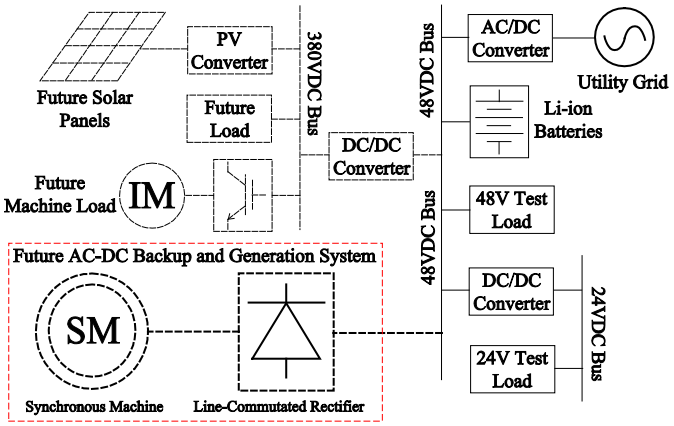

Fig. 1. A typical ac-dc microgrid system presently installed (solid lines) and to be further developed (dashed lines) in the Kaiser Building at the University of British Columbia, Vancouver, Canada [1].

time-phasor representations [9]−[17]. Defined as the envelopes of analytic signals [9], one type of DPs are able to down-shift the frequency spectra from around the 60 Hz fundamental frequency to 0 Hz [thus referred to as shifted-frequency analysis (SFA-type) DPs], and have been proven to offer effective simulations with flexible selection of step sizes [10]−[12]. Nevertheless, the SFA-type DPs are only applicable to modeling traditional ac power system components where the fundamental frequency is dominant.

To account for high-order harmonics that are generally of interest in ac-dc microgrid systems, this paper considers another type of DPs, which is based on the generalized averaging method (GAM) [13]. The GAM-type DPs allow the user to select desired modeling accuracy, thus are suitable for simulating ac-dc systems including various power electronic devices [13]−[17]. Finally, to take advantage of existing DP models [11], [17], an interface between the SFA- and GAM-type DPs is presented. Therein, the SM is modeled with SFA-type DPs as a 60 Hz power source using a voltage-behind-reactance (VBR) formation [18], and the LCR is modeled in GAM-type DPs for inclusion of desired harmonics.

The contributions of this paper are summarized as follows: 1) a new interface between the SFA- and GAM-type DPs is proposed; 2) the proposed interface allows for modeling of ac-dc power systems including the dc dynamics as well as the main harmonics of ac systems; 3) the proposed DP modeling approach is shown to accurately predict the responses of ac-dc systems, while yielding considerably improved efficiency over the time-domain detailed models.

978-1-5090-4168-8/16/$31.00 ©2016 IEEE

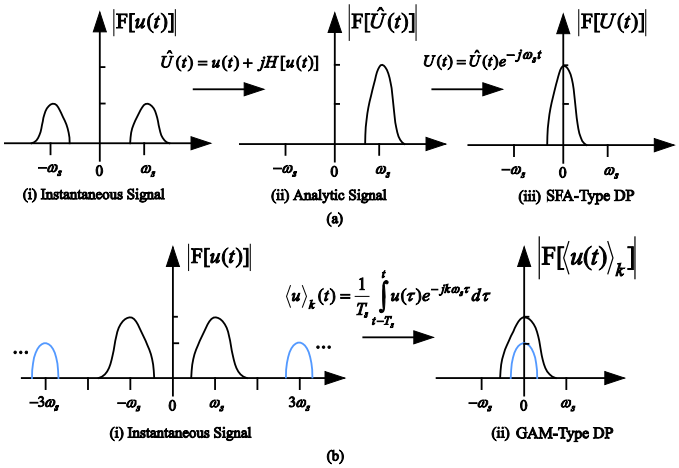

Fig. 2. Frequency spectra of the power system signal in different representations in the process of deriving: a) SFA- and b) GAM- type DPs.

II. DP Modeling Approaches

To set the stage for following discussions, a brief review of the SFA- and GAM-type DP definitions is first included.

A. Shifted-Frequency Analysis (SFA-type)

In power system dynamics analysis, the time-domain instantaneous signal $u(t)$ typically has a bandpass spectrum around the fundamental frequency, herein assumed to be f_s = 60 Hz or $\omega_s = 2\pi f_s \approx 377$ rad/s. In signal processing, $u(t)$ can be alternatively represented by its analytical signal $\hat{U}(t)$ [9], as

$$\hat{U}(t) = u(t) + jH[u(t)], \tag{1}$$

where $H(\cdot)$ denotes the Hilbert transform [9]. The SFA-type DP $U(t)$ of the instantaneous signal $u(t)$ is then defined as the complex envelope of its analytical signal $\hat{U}(t)$ [10], given by

$$U(t) = \hat{U}(t)e^{-j\omega_s t} = \{u(t) + jH[u(t)]\}e^{-j\omega_s t}. \tag{2}$$

As shown by (2), the SFA-type DP $U(t)$ can be obtained by shifting the analytic signal $\hat{U}(t)$ by $-\omega_s$ from its original frequency, which is also visualized in Fig. 2 (a). Similarly, the instantaneous signal $u(t)$ can be readily retrieved from $U(t)$ as

$$u(t) = \Re[\hat{U}(t)] = \Re[U(t)e^{j\omega_s t}]. \tag{3}$$

B. Generalized Averaging Method (GAM-type)

Nevertheless, due to the bandpass signal limitation, the SFA-type DPs are not suitable to model high-frequency harmonics that generally exist in integrated ac-dc power systems. Alternatively, to represent a power system signal shown in Fig. 2 (b) comprising both fundamental frequency and high-order harmonics, its time-domain waveform is viewed over a sliding interval $T_s = 2\pi/\omega_s$, and can be expressed using Fourier series expansion [13] as

$$u(\tau) = \sum_{k=-\infty}^{\infty} \langle u \rangle_k(t) e^{jk\omega_s \tau}, \tag{4}$$

where $\tau \in (t - T_s, t]$. Here, $\langle u \rangle_k(t)$ is the k^{th} Fourier coefficient, which is also defined as the k^{th} order GAM-type DP, given by

$$\langle u \rangle_k(t) = \frac{1}{T_s} \int_{t-T_s}^{t} u(\tau) e^{-jk\omega_s \tau} d\tau. \tag{5}$$

As seen from (4)-(5), the GAM-type DPs enable the user to select a number of Fourier coefficients (i.e., selection of k), to construct an adequate approximation of the original time-domain instantaneous signal.

C. Discussion of Methods

In summary, the process of deriving the SFA- and GAM-type DPs is shown in Fig. 2, wherein the DPs are obtained as analogous low-pass representations of the instantaneous signal. According to sampling theorem, the use of such low-pass DPs can be particularly helpful to achieve a significant reduction of the number of necessary time-steps compared to the original high-frequency signals [10].

Several aspects of the SFA- and GAM-type DPs are then summarized in Table I. Therein, for better illustration, the dynamic equations governing a series *R-L* circuit in different signal representations are also included. As shown in Table I, both the SFA- and GAM-type DPs closely resemble the conventional phasor [19], with difference being the time-derivative terms. Specifically, the conventional phasor and SFA-type DPs yield steady-state solutions as the envelopes of time-domain waveforms [10]. Also, the 1st order GAM-type DP (i.e. k =1 for fundamental frequency) is of half the magnitude of conventional phasor or SFA-type DP [13], which can be observed in (4)–(5) and in Fig. 2.

III. DP Modeling of System Components

For the purpose of this paper, a detailed model circuit diagram of the considered ac-dc backup generation system is depicted in Fig. 3. Therein, a constant-parameter VBR formulation of SM [18] is considered assuming ungrounded stator windings, M damper windings in q-axis, and N damper windings plus a field winding in the d-axis. The three-phase six-pulse LCR is then directly connected to the SM; and the dc filter consists of R_f, L_f, and C_f. More detailed modeling of this circuit configuration can be found in [2]−[3].

TABLE I
Aspects of Different Representations of Power System Signals

Representation	Type of signal	Assumption	Accuracy	Equation governing the *R-L* circuit
Instantaneous Signal	Time-Domain	n/a	Accurate	$v(t) = Ri(t) + L\frac{d}{dt}i(t)$
Conventional Phasor	Frequency-Domain	Quasi-Steady-State [19]	Low	$\mathrm{V}(\omega_s) = (R + j\omega_s L)\mathrm{I}(\omega_s)$
SFA-Type DP [10]	Hybrid Time-Phasor	Bandpass Signal	Accurate	$V(t) = (R + j\omega_s L)I(t) + L\frac{d}{dt}I(t)$
GAM-Type DP [13]	Hybrid Time-Phasor	Wideband Signal	Approximated with Desired Frequencies	$\langle v \rangle_k(t) = (R + jk\omega_s L)\langle i \rangle_k(t) + L\frac{d}{dt}\langle i \rangle_k(t)$

978-1-5090-4168-8/16/$31.00 ©2016 IEEE

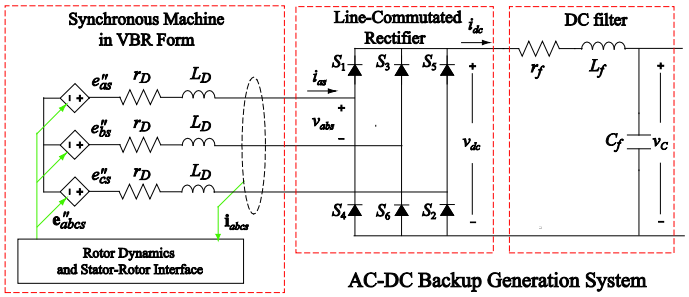

Fig. 3. Circuit diagram of the ac-dc backup generation system.

A. SFA-Type DP Modeling of SMs (SFA-SM)

To take advantage of existing DP models, the SFA-based SM model is considered [11] which consists of two parts: the stator equation in SFA-type DPs, and the rotor dynamics and interface expressed in time-domain *qd* coordinates.

1) Stator Equation

Since the VBR formulation offers a constant-parameter *R-L* stator circuit structure [18] as shown in Fig. 3, the stator equation is represented in SFA-type DPs as [11]

$$\mathbf{V}_{abcs} = \mathbf{L}''_D \cdot \frac{d}{dt}\mathbf{I}_{abcs} + [\mathbf{R}_D + j\omega_s \mathbf{L}''_D]\mathbf{I}_{abcs} + \mathbf{E}''_{abcs}, \tag{6}$$

where $\mathbf{V}_{abcs}$ and $\mathbf{I}_{abcs,}$ are the SFA-type DPs of stator voltages and currents, respectively; and

$$\mathbf{R}_D = diag(r_D, r_D, r_D);\ \mathbf{L}_D = diag(L_D, L_D, L_D), \tag{7}$$

where

$$r_D = r_s;\ L_D = L_{ls} + L''_{md}. \tag{8}$$

2) Rotor Dynamics and Interface

The subtransient voltage sources $\mathbf{E}''_{abcs}$ in (6) are given by

$$\mathbf{E}''_{abcs} = \mathbf{K}_{u,qd}^{U,abc}[e''_q \quad e''_d]^T, \tag{9}$$

where $\mathbf{K}_{u,qd}^{U,abc}$ can be found in [11], and

$$e''_q = \frac{L''_{md} + L_{ls}}{L''_{mq} + L_{ls}}\left\{\omega_r[\lambda''_d - (L''_{mq} - L''_{md})i_{ds}] + \sum_{j=1}^{M}\frac{L''_{mq} r_{kqj}}{L^2_{lkqj}}(\lambda_{mq} - \lambda_{kqj})\right\} + \frac{L''_{mq} - L''_{md}}{L''_{mq} + L_{ls}}(v_{qs} - r_s i_{qs}) \tag{10}$$

$$e''_d = -\omega_r \lambda''_q - \omega_r(L''_{mq} - L''_{md})i_{qs} + \sum_{j=1}^{N}\frac{L''_{md} r_{kdj}}{L^2_{lkdj}}(\lambda_{md} - \lambda_{kdj}) + \frac{L''_{md} r_{fd}}{L^2_{lfd}}(\lambda_{md} - \lambda_{fd}) + \frac{L''_{md}}{L_{lfd}}v_{fd}. \tag{11}$$

Due to the relatively slow electromechanical dynamics, the rotor state equations can be retained in *qd* coordinates in time domain as

$$\frac{d}{dt}\lambda_{kqj} = -\frac{r_{kqj}}{L_{lkqj}}(\lambda_{kqj} - \lambda_{mq}), \quad j = 1, \cdots M, \tag{12}$$

$$\frac{d}{dt}\lambda_{kdj} = -\frac{r_{kdj}}{L_{lkdj}}(\lambda_{kdj} - \lambda_{md}), \quad j = 1, \cdots N, \tag{13}$$

$$\frac{d}{dt}\lambda_{fd} = -\frac{r_{fd}}{L_{lfd}}(\lambda_{fd} - \lambda_{md}) + v_{fd}. \tag{14}$$

where λ_{kqj}, λ_{kdj}, and λ_{fd} are the rotor flux linkages, and the magnetizing flux linkages are given by

$$\lambda_{mq} = L''_{mq} i_{qs} + \lambda''_q;\ \lambda_{md} = L''_{md} i_{ds} + \lambda''_d. \tag{15}$$

Here, the inductances L''_{md} and L''_{mq} are defined as

$$L''_{mq} = \left(\frac{1}{L_{mq}} + \sum_{j=1}^{M}\frac{1}{L_{kqj}}\right)^{-1};\ L''_{md} = \left(\frac{1}{L_{md}} + \frac{1}{L_{fd}} + \sum_{j=1}^{N}\frac{1}{L_{lkdj}}\right)^{-1}, \tag{16}$$

and the subtransient flux linkages are

$$\lambda''_q = L''_{mq}\left(\sum_{j=1}^{M}\frac{\lambda_{kqj}}{L_{lkqj}}\right);\ \lambda''_d = L''_{md}\left(\frac{\lambda_{fd}}{L_{lfd}} + \sum_{j=1}^{N}\frac{\lambda_{kdj}}{L_{lkdj}}\right). \tag{17}$$

Finally, the transformation for stator currents is similar to (3)

$$\mathbf{i}_{qd0s} = \mathbf{K}_s \Re[\mathbf{I}_{abcs} e^{j\omega_s t}]. \tag{18}$$

B. GAM-Type DP Modeling of LCRs (GAM-LCR)

DP modeling the ac-dc dynamics of the LCR, however, can be more complex since it can introduce significant harmonics into the systems. Typically, for system-level studies the GAM-type DP modeling has been used with inclusion of the first few dominant harmonics [13]−[17]. This paper then considers the GAM-type DP modeling of LCRs based on modulation theory [16]−[17], which relates the ac- and dc-side DPs as

$$\langle \mathbf{i}_{abcs} \rangle_k = \langle i_{dc} \cdot \mathbf{s}_{iabc} \rangle_k = \langle i_{dc} \rangle_0 \langle \mathbf{s}_{iabc} \rangle_k, k \in K, \tag{19}$$

$$\langle v_{dc} \rangle_0 = \langle v_{as} \cdot s_{va} \rangle_0 + \langle v_{bs} \cdot s_{vb} \rangle_0 + \langle v_{cs} \cdot s_{vc} \rangle_0 = \sum_{k \in K} 2 \cdot \mathrm{Re}\left[\langle v_{as} \rangle_k \langle s_{va} \rangle_k^* + \langle v_{bs} \rangle_k \langle s_{vb} \rangle_k^* + \langle v_{cs} \rangle_k \langle s_{vc} \rangle_k^*\right] \tag{20}$$

Here, the vectors $\langle \mathbf{v}_{abcs} \rangle_k$ and $\langle \mathbf{i}_{abcs} \rangle_k$ are the GAM-type DPs of the ac voltages and currents, respectively, and *k* denotes the selected harmonic order of the corresponding DPs. Since the dc filter is included, only the 0th order DPs $\langle v_{dc} \rangle_0$ and $\langle i_{dc} \rangle_0$ are modeled for dc variables. Additionally, $\langle \mathbf{s}_{vabcs} \rangle_k$ and $\langle \mathbf{s}_{iabcs} \rangle_k$ are the voltage and current switch functions based on Fourier-series-approximation [17], [20], which can be expressed as

$$\begin{cases} \langle s_{va} \rangle_k = \frac{A_k}{2}\cos(\frac{k\mu}{2})e^{j(0)} \\ \langle s_{va} \rangle_k = \langle s_{vb} \rangle_k e^{j(\frac{2k\pi}{3})} = \langle s_{vc} \rangle_k e^{j(\frac{-2k\pi}{3})} \end{cases}, k \in K, \tag{21}$$

$$\begin{cases} \langle s_{ia} \rangle_k = \frac{A_k}{k\mu}\sin(\frac{k\mu}{2})e^{j(0)} \\ \langle s_{va} \rangle_k = \langle s_{ib} \rangle_k e^{j(\frac{2k\pi}{3})} = \langle s_{ic} \rangle_k e^{j(\frac{-2k\pi}{3})} \end{cases}, k \in K, \tag{22}$$

where

$$A_k = \frac{4}{k\pi}\sin(\frac{k\pi}{2})\cos(\frac{k\pi}{6}), \tag{23}$$

and the commutation angle μ is calculated as

$$\mu = \cos^{-1}(1 - \frac{\sqrt{2}\omega_s L_D \langle i_{dc} \rangle_0}{V_{line}}). \tag{24}$$

C. DC Subsystem Modeling

Similar to rotor variables, the dc subsystem dynamics are slow-changing. Considering (4)−(5), when $k = 0$, $\langle u \rangle_0(k)$ degrades to dynamic averaging in time-domain. Therefore, the dc subsystems can be modeled directly in time-domain.

978-1-5090-4168-8/16/$31.00 ©2016 IEEE

IV. The Proposed DP Interface

To interconnect the discussed component models, the ac-dc backup generation system can be implemented using the DP interface depicted in Fig. 4. For the purpose of this paper, the dominant 1st, 5th, and 7th harmonics in the six-pulse LCRs are investigated, i.e., $K = \{1, 5, 7\}$. As shown in Fig. 4, the GAM-LCR model can be interfaced to the ac system comprising a number of subsystems for the fundamental frequency and each of the harmonics. In particular, in the 1st order DP subsystem the SFA-SM model is viewed as a controlled VBR power source (with magnitude adjustment); for 5th, and 7th order DPs, it is assumed that zero voltage source is provided. Finally, the dc subsystem is modeled directly in time-domain as discussed in Section III–C. It is also noted that such proposed DP interface can be readily augmented to include higher-order harmonics of interest, provided that the dynamics at these frequencies are significant or desired.

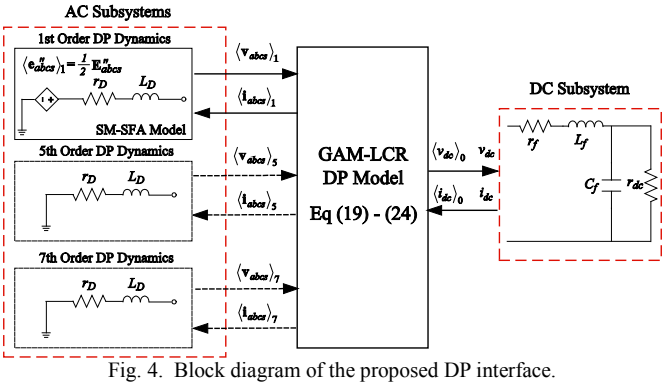

Fig. 4. Block diagram of the proposed DP interface.

V. Computer Studies

The ac-dc backup generation system studied here is the same as in [2]−[3], which has been validated with detailed simulations and experimental measurements. The proposed DP model is implemented in MATLAB/Simulink [4]−[5], and the detailed switch-level model shown in Fig. 3 has been implemented in PLECS toolbox [7] and is used as benchmark.

In the following studies, the system initially operates in steady state with a constant excitation E_{xfd} =19.5 V and an equivalent dc load resistance r_{dc} = 21 Ω connected to the dc filter output; at t = 0.1 s, the dc load resistance is changed to r_{dc} = 3.64 Ω; and the simulation is run until t = 0.5 s for the system to reach a new steady-state condition.

A. Small Step Sizes Study

To validate the modeling accuracy, the system is first solved using ode23tb solver [4] with the following settings: relative and absolute error tolerances of 10^{-4}, and maximum and minimum step sizes of 100 μs and 0.1 μs, respectively.

Due to space constraint, only the responses of phase a and dc voltages and currents as predicted by the subject models (i.e., the detailed and DP models) are shown in Fig. 5. Three fragments of Fig. 5 showing the pre-, during, and post- load change system responses are also magnified and shown in Fig. 6. In both Figs. 5 and 6, the resulting DP trajectories $\langle v_{as} \rangle_k$ and $\langle i_{as} \rangle_k$ have been converted to their time-domain instantaneous values v_{as} and i_{as} using (4). In addition, to better

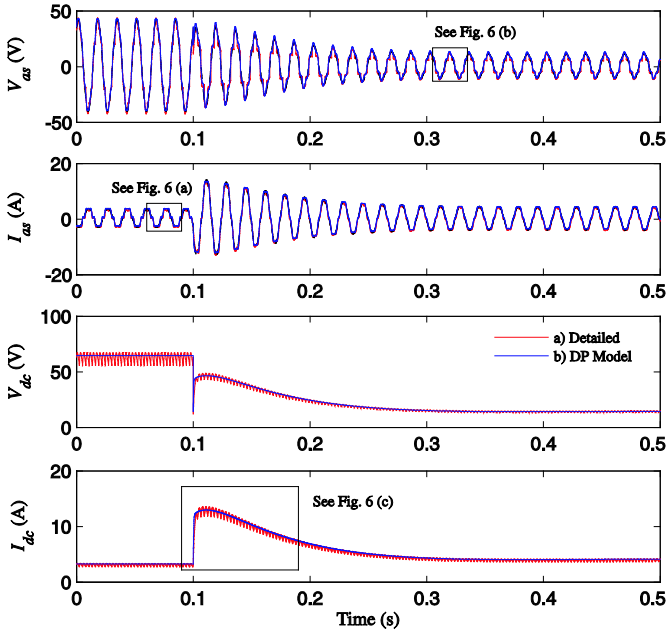

Fig. 5. System response to a load change as predicted by the subject models.

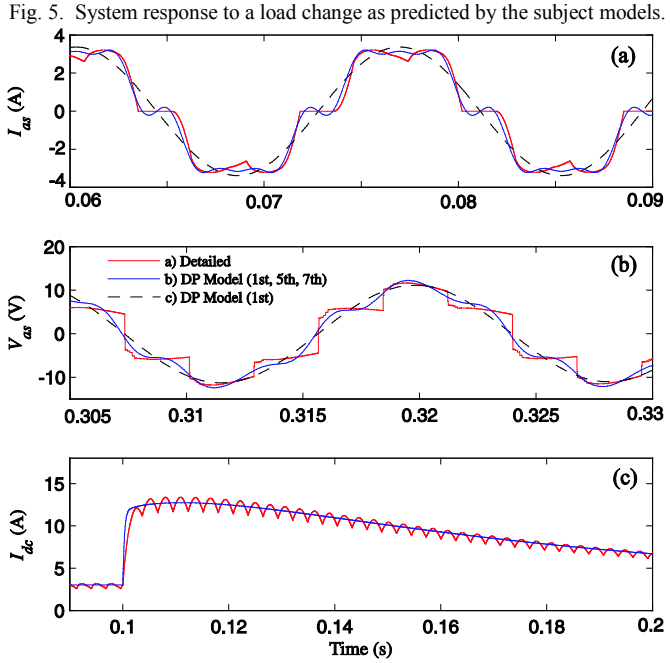

Fig. 6. Magnified view of the ac and dc variables as depicted in Fig. 5: (a) i_{as} in the original steady state; (b) v_{as} in the new steady state; and (c) i_{dc} during the load-change transient.

illustrate the adjustable modeling accuracy of GAM-type DPs, the ac-side responses predicted with only the 1st order DPs, i.e., $K = \{1\}$, are plotted as the dashed line [see line c)].

As can be seen in Figs. 5 and 6, the detailed and DP models yield consistent ac and dc results. In particular, by including the 5th and 7th major harmonics, the DP model is capable of producing results well matched to those predicted by the detailed model [see lines a) and b)]. When only the 1st order DP is modeled, v_{as} and i_{as} demonstrate the fundamental frequency components. For the dc-side, the $\langle v_{dc} \rangle_0$ and $\langle i_{dc} \rangle_0$ results are obtained as dynamic averaging values as previously discussed. It is also noted that the DP model solution in Fig. 6

978-1-5090-4168-8/16/$31.00 ©2016 IEEE

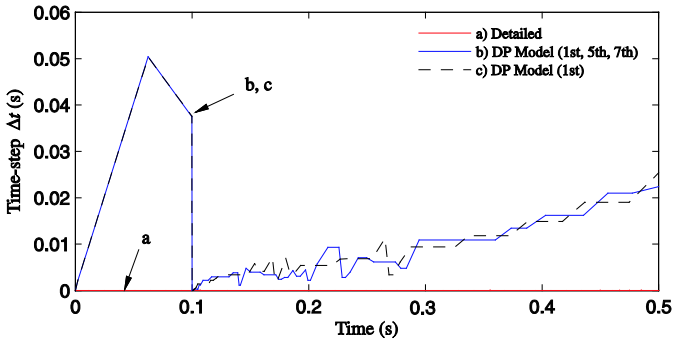

Fig. 7. Step size Δt as chosen by the subject models.

TABLE II
SIMULATION EFFICIENCY OF THE SUBJECT MODELS

Model	No. of Time Steps	CPU Time, ms
Detailed	42198	1553.9
DP (1st, 5th, 7th)	153	85.7
DP (1st)	144	43.8

(c) exhibits certain difference at the beginning of load-change transient, and converges to the detailed solution very quickly. This is due to the inclusion of the stator inductances L_D into the commutation angle μ [see (24)], which simplifies the stator circuit blocks to be purely algebraic (thus less fast-transient details).

B. Flexible Step Sizes Study

Next, the case study is solved using the same settings but with a maximum step size of 0.1s, which allows the solver to adaptively select the step size on-the-fly. To focus on the numerical efficiency performance, the step size Δt of the subject models is depicted in Fig. 7 as a function of time. As shown in Fig. 7, the step sizes of the detailed model remain relatively small during the whole simulation period, as seen adjacent to the horizontal axis. In contrast, the Δt curves of DP models start at large values, drop at the load-change instance, and then start raising again rapidly, which reflect the system modes as it starts in steady state, encounters and then recovers from a disturbance. The system response of ac and dc variables in this case are similar to Figs. 5 and 6 (except at much larger time steps), and therefore are not included here.

Finally, a quantitative assessment of the simulation efficiency of the subject models is summarized in Table II. It is seen that the DP models require at least three orders of magnitude fewer time steps than the detailed model (153/144 versus 42918 steps) due to the use of DPs. Consequently, the DP models significantly outperform the detailed model in terms of CPU time (85.7/43.8 versus 1553.9 ms). Due to simpler modeling complexity, the DP model using only 1st order DPs also requires less CPU time than the one including higher-order harmonics.

VI. CONCLUSIONS

In this paper, the DP modeling of ac-dc backup generation system has been proposed using an interface between SFA- and GAM-type DPs. Therein, the SM is modeled as a 60 Hz VBR source using SFA-type DPs, and the LCR is modeled in GAM-type DPs for inclusion of desired harmonics. The proposed DP model is shown to produce simulation results including both fundamental frequency components and harmonics well matched to those predicted by the time-domain detailed model. The computer studies demonstrate that the proposed DP model effectively works with variable-step solvers, and can significantly reduce the CPU time compared to the detailed model. This approach may be a numerically efficient way of modeling the future integrated ac-dc power systems.

REFERENCES

[1] University of British Columbia (2014). UBC's Living Lab Report [Online]. Available: https://sustain.ubc.ca/our-commitment/campus-living-lab

[2] S. D. Sudhoff, K. A. Corzine, H. J. Hegner, and D.E. Delisle, "Transient and dynamic average-value modeling of synchronous machine fed load-commutated converters," *IEEE Trans. Energy Convers.,* vol. 11, no.3, pp. 508-514, Sep. 1996.

[3] O. Wasynczuk and S.D. Sudhoff, "Automated state model generation algorithm for power circuits and systems", *IEEE Trans. Power Syst.,* vol. 11, no.4, pp. 1951-1956, Nov. 1996.

[4] *MATLAB 7 (R2014b)*, The MathWorks Inc., Natick, MA, USA, 2014.

[5] *Simulink– User's Manual,* The MathWorks, Inc., Natick, MA, 2012.

[6] *SimPowerSystems User Guide*, The MathWorks, Inc., Natick, MA, 2014.

[7] *Piecewise linear electrical circuit simulation (PLECS) User Manual*, version. 3.7, Plexim GmbH, Zurich, Switzerland, 2015.

[8] *PASCAD X4 Online Help,* version. 4.5.2, Manitoba HVDC Research Centre, Winnipeg, MB, Canada, 2013.

[9] S. Henschel, "Analysis of electromagnetic and electromechanical power system transients with dynamic phasors", Ph.D. dissertation, Univ. British Columbia, Vancouver, BC, Canada, 1999.

[10] P. Zhang, J. R. Marti, and H. Dommel, "Shifted-frequency analysis for EMTP simulation of power-system dynamics," *IEEE Trans. Circuits Syst.* I: Reg. Papers, vol. 57, no. 9, pp. 2564–2574, Sep. 2010.

[11] Y. Huang, M. Chapariha, F. Therrien, J. Jatskevich, and J. Marti, "A constant-parameter voltage-behind-reactance synchronous machine model based on shifted-frequency analysis," *IEEE Trans. Energy Convers.,* vol. 30, no.2, pp. 761-771, Jun. 2015.

[12] Y. Huang, F. Therrien, J. Jatskevich, and L. Dong, "State-space voltage-behind-reactance modeling of induction machines based on shifted-frequency analysis," in *IEEE Power and Energy Society General Meeting (PES-GM),* Denver, USA, 2015.

[13] S. R. Sanders, J. M. Noworolski, X. Z. Liu, and G. C. Verghese, "Generalized averaging method for power conversion circuits," *IEEE Trans. Power Electron*., vol. 6, pp. 251–259, Apr. 1991.

[14] T. H. Demiray, "Simulation of power system dynamics using dyanmic phasors models," Ph.D. dissertation, Swiss Fed. Inst. Technol., Zurich, Switzerland, 2008.

[15] A. M. Stankovic, and T. Aydin, "Analysis of asymmetrical faults in power systems using dynamic phasors," *IEEE Trans. Power Syst.* , vol. 15, no. 3, pp. 1062-1068, Aug. 2000.

[16] M. Daryabak, S. Filizadeh, J. Jatskevich, A. Davoudi, M. Saeedifard, V.K. Sood, J. A. Martinez, D. Aliprantis, J. Cano, and A. Mehrizi-Sani, "Modeling of LCC-HVDC systems using dynamic phasors," *IEEE Trans. Power Del.,* vol. 29, no.4, pp. 1989-1998, Aug. 2014.

[17] C. Liu, A. Bose, and P. Tian, "Modeling and analysis of HVDC converter by three-phase dynamic phasor," *IEEE Trans. Power Del.,* vol. 29, no.1, pp. 3-12, Feb. 2014.

[18] M. Chapariha, F. Therrien, J. Jatskevich, and H. W. Dommel, "Explicit formulations for constant-parameter voltage-behind-reactance interfacing of synchronous machine models," *IEEE Trans. Energy Convers.,* vol. 28, no.4, pp. 1053-1063, Dec. 2013.

[19] P. Kundur, *Power System Stability and Control.* New York: McGraw-Hill, 1994.

[20] L. Hu, and R. Yacamini, "Harmonic transfer through converters and HVDC links," *IEEE Trans. Power Electron.,* vol. 7, no. 3, pp. 514-525, Jul. 1992.

978-1-5090-4168-8/16/$31.00 ©2016 IEEE